Research Article

Abrasion Resistance and Water Absorption Characteristics of Ti-HAp Hybrid Reinforced Polyetheretherketone Biocomposites

Agbeboh Newton Itua*
Department of Mechanical and Mechatronics Engineering, Federal University Otuoke, Bayelsa State, Nigeria

Oladele Isiaka Oluwole and Daramola Oluyemi Ojo
Department of Metallurgical and Materials Engineering, Federal University of Technology, Ondo State, Nigeria

Adegun Miracle Hope
Department of Mechanical and Aerospace Engineering, The Hong Kong University of Science and Technology, Hong Kong

* Corresponding author. E-mail: agbebohni@fuotuoke.edu.ng DOI: 10.14416/j.asep.2023.02.005
Received: 31 August 2022; Revised: 9 December 2022; Accepted: 13 January 2023; Published online: 6 February 2023

Abstract
The influence of abrasion on biomedical implant in human body is a constant cause of pain, discomfort and sometimes a repeat of surgery as a result of the complications from the effects of wear on the implants and the negative consequences of the resultant abrasive particles on the surrounding tissue and bodily environment. To alleviate this, a titanium-hydroxyapatite hybrid reinforced polyetheretherketone (PEEK) biocomposite material was developed, characterized and tested. X-Ray Diffraction characterization revealed that the calcined eggshell was composed mainly of lime and portlandite. The calcined eggshell was then used in the synthesis of hydroxyapatite powder (HAp) with characteristic bands confirmed by FTIR spectroscopic analysis. Biocomposites were developed from the blend of titanium and hydroxyapatite powders in varying proportions as reinforcements in PEEK matrix. The developed composites and control sample were subjected to abrasion and water absorption tests from where it was revealed that biocomposite sample reinforced with 10 wt.% orthophosphoric acid synthesized eggshell possess optimum abrasion resistance with a wear index of 0.20 mg/cycle with an acceptable level of water absorption next to the unreinforced polyetheretherketone over a period of 35 days.

Keywords: Biomedical implant, Abrasion resistant, Bone necrosis, Hydroxyapatite, Titanium

1 Introduction

The human body is subject to different modes of failure as a result of several factors including accidents, diseases and aging. These failures or damages usually result in the impairment of human tissues. These damaged tissues may either be repaired by healing and regrowth or they may require outright replacement by tissue transplant or other suitable methods [1]. The acquisition of suitable human tissue replacement materials is quite challenging due to the unique nature of the human body [2]. As a result of this, numerous medical experts have attempted to replace ailing parts of the human body with various materials including metals, polymers, ceramics, wood, and other materials with limited success [3]. Subpar implant performance or implant failure could result in significant worsening of the ailments or some instances even be fatal. Consequently, this has necessitated an increase in research into the acquisition and development of better biomaterial replacement for failed human tissues.

Numerous materials are currently utilized for implant development, including ceramics, polymers, metals and composites. These implants are chiefly

used in orthopedic surgeries, each with different effects, which can be both advantageous and detrimental. Occasionally, these detrimental effects result in serious issues including imperfect osteogenesis, stress-shielding and others. Many of these issues are so serious that they could even require repeat surgery immediately after implantation or a short while after. A repeat surgery is most times very painful and inconvenient, it is, therefore, not very suitable for old or weak patients as it constitutes a considerable risk to the patient's life. This makes the development of a material with considerably better properties a necessity. It is vital that the properties of any implant material must closely match that of the bone it is replacing, to avoid or limit the detrimental effects and issues that could result in worsening of the affected parts and subsequent re-fractures or re-surgeries [4].

Generally, implants used for load bearing in everyday life must possess high fatigue strength, while implants used in teeth and joints must have high hardness and wear resistance. Metals are currently one of the most promising for these biomaterials. They are used as replacements for human hard tissues due to their high strength and durability. Although, several disadvantages including corrosion, stress shielding and radiological interferences ensue from the use of metals. Numerous research efforts have culminated in the development of specialized metals and alloys that significantly reduce these disadvantages while enhancing the advantages like strength and durability. Examples of these metallic materials are titanium, stainless steels, cobalt alloys and titanium alloys. Several other materials including metal alloys, ceramics, polymers and composites have been investigated and studied. These studies have resulted in steady improvements in the development of implants and prosthetic materials, for the replacement of damaged human tissues over the years [5], [6].

The use of titanium for the development of prosthetic materials and implants is largely attributed to its lightweight, biocompatibility, strength and low elastic modulus. Consequently, titanium is one of the few naturally occurring materials that meet the requirements for the development of implantable biomaterial components. The main titanium variants commonly used in biomedicine are commercially pure titanium grade 2 (cp-Ti G2) and Ti-6Al-4V (grade 5) alloy, commonly used in the manufacture of dental, bone, joints and other hard tissue replacements. However, its application is hindered by its low resistance to abrasion due to its severe adhesive wear and high friction coefficient. Several methods have been investigated to improve the osseointegration and tribological properties of titanium, including surface modification techniques with promising results [7].

Polyetheretherketone (PEEK) is a synthetic, semi-crystalline, linear polycyclic, aromatic, biocompatible, thermoplastic polymer. It has a similar elastic modulus to human cortical bone, making it ideal for human load bearing and motility related implant applications [4]. Its properties are determined by the unique chemistry, architecture and bonding of the constituent molecules, which make up the polymer backbone and the mode and extent of intermolecular solidification upon polymer formation [8]. The morphological changes that occur upon thermal exposure also influence the properties of the developed PEEK polymer. PEEK possesses superior sterilization resistance and chemical stability at high temperatures as well as radiolucency, which makes it very useful for fabricating spinal fusion implant devices. This relationship must be taken into account when manufacturing and fabricating parts for different applications [9]. The most common applications for PEEK biomaterials include arthroplasty and arthroscopic implant devices, spinal fusion cages, interference screws, joint bearing devices, suture anchors and 3D printed patient specific implants. It has been observed that PEEK implants have comparable or somewhat superior clinical performances than other polymers including Ultra High Molecular Weight Poly-Ethylene (UHMWPE) and even metals. However, despite its numerous advantages, high cost, low surface energy and relatively hydrophobic surface which limits cellular adhesion, lack of thermoformability and its complexity are some of the major limitations with its use in the development of biomaterial implants [10], [11], [12].

Hydroxyapatite is a bioceramic calcium phosphate-based material having a mineral phase similar to that of the human bone. In its pure state hydroxyapatite is composed of about 57% phosphorus, 40% calcium and 2% hydroxyl ions [13]; thereby, enhancing biocompatibility, bioactivity and reactivity within the human body environment [14]. It is a considerably brittle ceramic material with a hexagonal

or monoclinic crystal structure that permits the substitution of replacement ions into its chemical structure. Consequently, hydroxyapatite is not as strong as the human bone or most other conventional implant materials and cannot be used as a standalone implant material. Conversely, most materials in nature are also not as bioactive and cannot integrate well with adjacent bone tissues or trigger tissue regrowth. Hydroxyapatite can be obtained from different sources including synthetic and natural sources, via different production processes with varying levels of complexity, and adverse effects on the environment. It is therefore imperative that hydroxyapatite is gotten from environmentally friendly and sustainable sources [1], [4]. Due to its exceptional biocompatibility hydroxyapatite, has been applied as a coating material or reinforcement in other stronger but less biocompatible materials, including titanium, Ti6Al4V, UHMWPE, PEEK, etc. [5].

Aside from the obvious concern about the biocompatibility of implant materials, the gap in strength between implant materials and human hard tissue is a very serious cause for concern, which must be bridged or significantly reduced for the implants to function well [15]. An imbalance in strength between the implant interface and the surrounding hard tissues commonly results in a phenomenon known as bone-implant interfacial abrasion, which refers to the propensity of biomaterial implants to wear out over time as a result of the interaction of the biomaterial implants with the surrounding soft or hard tissue within the human body. These interactions may result in implant fragmentation or degradation. Another common consequence of bone-implant interfacial wear or abrasion is bone necrosis, which occurs when the strength of the implant in contact with or used to replace human bone tissue is superior to that of the surrounding bone tissue, it is characterized by the gradual wearing off of pieces of bone tissue upon consistent and repetitive contact with the implant under the application of force, load or stress [16]. In some instances the implant is considerably stronger than the bone, the implant gradually and repeatedly crushes the bone tissue in contact with it into tiny and sometimes microscopic bits which pierce into and sometimes get stuck in the surrounding tissue, while the reverse is the case when the bone is significantly stronger than the implant, causing the implant to be crushed and stuck instead, this results in the injury of surrounding tissues, and other health complications [17]. To prevent bone necrosis there must be a balance in the strengths and properties of the natural human bone tissue and the supplementary implant material. This has created a need for novel abrasion-resistant materials, which are permeable to bodily fluids and still capable of allowing cell proliferation and subsequent bone growth. It is, therefore, highly imperative to carry out vigorous research to develop more suitable wear resistant materials for such implant applications, either by the creation of new and novel materials or improving upon those that already exist.

This research attempts to develop a material from the combination of novel mix of titanium and hydroxyapatite within a PEEK matrix and investigate its abrasive properties to ensure that it matches that of cortical bone during implant application or service to avoid necrosis and other adverse complications due to the pieces generated as a result of abrasion and implant mismatch.

2 Materials and Methods

2.1 *Materials*

The materials used for this study are cracked chicken egg shells from White Leghorn chicken breed procured as waste products from a farmland located at latitude 6°44'40.5"N and longitude 6°07'51.9"E in Ekpoma, Edo State, Nigeria. Ammonium Hydroxide ($(NH_4)OH$), analytical grade 99% pure Orthophosphoric acid (H_3PO_4), and Teflon sheets, obtained from Pascal Chemicals Akure, Nigeria. Ames Tests B5051 Muta-ChromoPlate™ Bacterial Strain Kit (2 Strain Kit) Kits were purchased from Environmental Bio-Detection Products Inc. (EBPI), 735 Griffith Court, L7L 5R9, and 6800 Campobello Rd, Mississauga, L5N 2L8, Ontario Canada. Titanium powder with chemical composition was used as reinforcement in combination with hydroxyapatite (Table 1).

It was certified grade 2 (Gr2) with 99.6% purity by Baoji Lihua Non-ferrous Metals Co., Ltd. Taicheng Road, Baoji City, Shaaxi Province, China. The titanium powder was of a 400 mesh sieve passing and a dark coloration. PEEK of series 450G with properties shown in Table 2 was procured from Jiangsu Junhua High Performance Specialty Engineering Plastics

Products Co., Ltd. No. 377 South Wuyi Road, Creativity Industry Zone, Wujin District, Changzhou City, Jiangsu Province, China.

Table 1: Chemical composition of Gr2 titanium powder

Element	Percentage Composition (%)
Titanium (Ti)	99.6
Hydrogen (H)	0.023
Iron (Fe)	0.028
Oxygen (O)	0.35
Nitrogen (N)	0.011
Carbon (C)	0.010
Micah (Mi)	<0.01
Silicon (Si)	0.015
Chlorine (Cl)	0.02
Magnesium (Mg)	<0.01

2.2 *Procurement and processing of the eggshells*

Natural sourced hydroxyapatite was obtained via the processing of eggshells. The egg shells samples were prepared using processes described by [18], [5]. The materials were gathered together and meticulously cleaned to remove all the debris, sand and other impurities, after which the materials were washed using distilled water and sun-dried for 48 h. The materials were then sorted into batches, and boiled separately to remove the leftover organic materials and membranes, after which they were washed, cleaned, and dried in an oven at 80 °C for 24 h. The dried materials were mechanically crushed with a laboratory jaw crusher and pulverized to smooth powdery form using a laboratory ball mill operated at 300 rpm for 48 h to produce a fine granular material composed mainly of calcium carbonate ($CaCO_3$), which was sieved using a sieve with 90 µm aperture size to obtain powders with the required particle size of less than 90 µm. These calcium carbonate materials were weighed and put into sizeable ceramic crucibles and then charged into a muffle furnace. This was done to convert the materials to calcium oxide via a three-stage calcination process outlined in Table 3. To ensure complete conversion according to the process outlined by [5], [18], the crucibles containing the materials were placed in an electric muffle furnace and first heated from room temperature to 450 °C at a rate of 12 °C/min, the temperature was held constant for 1 h to ensure that all the organic material burns off and the smoke being emitted stops. Then secondly the materials were heated to 700 °C at a heating rate of 8 °C/min and held at this temperature for 2 h, to ensure all the proteins and organic elements were completely burnt off, and to begin the process of decarbonization and emission of CO_2 as shown via the chemical equation in Equations (1) and (2).

Table 2: PEEK Series 450G Properties and Data Sheet

Item	Unit	Test Standard or Instrument	100% PEEK450G
Color			Natural or Black
Density	g/cm^3	ISO 1183	1.3 ± 0.01
Water Abs. (25 °C.24 h)	%	ISO 62	0.5
Mould shrinking percentage	%	3 mm,170 °C, Flow direction	1.2
	%	Perpendicular to flow direction	1.5
Melting point	°C	DSC	343
Distortion temperature	°C	ASTM D648	163
Continuous using temperature	°C	UL 74685	260
Coefficient of thermal expansion	10–5/°C	ASTM D696	4.7
Tensile strength (23 °C)	MPa	ISO 527-2/1B/50	100
Tensile elongation (23 °C)	%	ISO 527-2/1B/50	34
Bending strength (23 °C)	MPa	ISO 178	163
Compressive strength (23 °C)	MPa	ASTM D695	118
Izod impact strength (no gap)	KJm^{-2}	ISO 180/U	No crack
Rockwell hardness	-	ASTM D785	99
Flammable level	V-0 @ mm	UL 94	1.5
Dielectric strength	KV/mm	IEC 248	1.8
Dielectric constant	-	IEC 250	-
Surface resistivity	Ω	-	1015 Ω
Friction coefficient	M	-	0.30–0.38

Table 3: Three-stage calcination temperature chart

Stage No.	Temp. Range (°C)	Heating Rate (°C/min)	Final Temp. (°C)	Soaking Time (h)	Effects Observed
1	25–450	12	450	1	Smoke indicates the burning off of the membranes and organic materials.
2	450–700	8	700	2	Decarbonization, CO_2 emission, organic compounds and protein burn off.
3	700–1000	4	1000	3	Complete decarbonization and transformation into calcium oxide CaO and calcium hydroxide $Ca(OH)_2$.

$$CaCO_3 + Heat \rightarrow CaO + CO_2 \quad (1)$$

$$CaO.H_2O \xrightarrow{Heat} Ca(OH)_2 \quad (2)$$

The third stage of calcination was carried out by heating the materials from 700 °C to 1000 °C at a heating rate of 4 °C/min and holding for 3 h to ensure complete calcination at about 900 °C, along with total decarbonization and transformation of the rhombohedral calcium carbonate ($CaCO_3$) within the eggshells to calcium oxide (CaO) and subsequently calcium hydroxide ($Ca(OH)_2$) when exposed to air.

The various structural phases present in the materials were confirmed by X-Ray Diffraction (XRD) and then the samples obtained were used in the synthesis of hydroxyapatite via wet chemical precipitation methods using two different sets of chemicals. The powders were divided into two sets of 500 g each, for the synthesis of hydroxyapatite via an orthophosphoric acid based wet chemical precipitation process.

2.3 *Hydroxyapatite powder synthesis using orthophosphoric acid*

After calcination, measurement and grouping into batches of 500 g each, 5 g of the CaO obtained were measured into three separate beakers each containing 100 mL of distilled water and subjected one after the other to the same orthophosphoric acid-based wet chemical precipitation process. Each beaker containing the solution was placed on a hot plate magnetic stirrer and allowed to boil while the solution was thoroughly stirred. The stirring was carried out continuously for 2 h and as the solution boiled an effervescent reaction was observed, signifying that CaO was being completely transformed to $Ca(OH)_2$ in accordance with the observation made by Bonou *et al.*, [19]. The reaction proceeded according to the chemical equation stated in Equation (3)

$$10CaO + 10H_2O \rightarrow 10Ca(OH)_2 \quad (3)$$

The solution was then reacted with 20 mL of 99% purity analytical grade orthophosphoric acid (H_3PO_4) while stirring at 120 rpm according to the processes outlined by [6]. A suspension of precipitates was initially observed, which dissolved upon further stirring, for about 30 min after which the precipitates were completely dissolved into the solution. The pH of the solution was kept constantly below 2 by the dropwise addition of 1 M ammonium hydroxide (NH_4OH) solution when needed. After all the precipitates had dissolved, indicating the completion of the reaction, stirring was stopped, the beaker was removed from the heating medium and allowed to cool and age for 7 days according to the processes outlined by [15]. Equation (4) shows the chemical equation for the reaction.

$$10Ca(OH)_2 + 6H_3PO_4 \rightarrow Ca_{10}(PO_4)_6(OH)_2 + 18H_2O \quad (4)$$

After aging, the solution was filtered using filter paper and the residue was oven-dried at 105 °C for 1 h. The dried residue was then put in a crucible and transferred to a furnace where it was subjected to heat treatment in three stages, first by heating to 425 °C at a heating rate of 5 °C/min, secondly by heating to 700 °C at a heating rate of 10 °C/min, and then finally heating to 1000 °C at a heating rate of 15 °C/min and holding for 3 h. Table 4 summarizes this process of heat treatment which caused the HAp to crystallize and undergo sintering to form dendrites, which agglomerated into lumps. The samples were allowed to cool in the furnace and thereafter removed and the lumps formed were then pulverized using a laboratory jaw crusher and milled to powder using a ball mill with steel balls. The powdered particles were then subjected to sieve analysis after grinding to determine the particle size, and particles of 90 μm sieve aperture passing were obtained.

Table 4: Calcination temperature chart for the HAp powders derived using orthophosphoric acid

Stage No.	Temp. Range (°C)	Heating Rate (°C/min)	Final Temp. (°C)	Soaking Time (h)	Effects Observed
1	25–425	5	425	0	Boiling of the chemicals and slight smoking as the fumes from the chemicals evaporate and due to emission of gases, gradual transformation to solution as the temperature increases.
2	425–700	10	700	0	Slight boiling and fume emission due to the release of gases upon heating, leaving a slightly agglomerated, red hot, gelatinous substance.
3	700–1000	15	1000	3	Total liquefaction of sample and upon cooling the sample is transformed to hard sintered whitish solid.

The full chemical reaction of the complete process is adjusted in Equation (5) to show the reaction between CaO and water to form calcium hydroxide, and the precipitation of hydroxyapatite upon reaction with orthophosphoric acid:

$$10CaO + 10H_2O + 6H_3PO_4 \rightarrow Ca10(PO_4)_6(OH)_2 + 18H_2O \quad (5)$$

Equation (5) is, therefore, the expected chemical equation for the synthesis of hydroxyapatite using orthophosphoric acid-based wet chemical precipitation method. The resultant hydroxyapatite material was confirmed using XRD and FTIR, the process was used to convert the remaining 500 g of CaO to hydroxyapatite, which was further confirmed using XRD and FTIR analysis. After the synthesis and characterization, the samples were used as reinforcement materials along with titanium in the production of composite biomaterials. Hydroxyapatite powders were synthesised using chemical reagents including ammonium hydroxide ($(NH_4)OH$), and analytical grade 99% pure orthophosphoric acid (H_3PO_4). After synthesis the HAp powders were characterised and analysed and the results shown and discussed.

2.4 *Composite development*

The hydroxyapatite powders derived from the Orthophosphoric Acid Wet Chemical Precipitated Eggshells (OA-ES) were combined with titanium powders and used as reinforcement within PEEK matrix to develop hybrid composites. The powder reinforcements were added to the PEEK matrix in predetermined proportions of 5, 10, 15, 20, 25 and 30 wt.% and stirred continuously at 1400 rpm using a magnetic stirrer for 10 min to obtain a homogeneous mixture. The homogenous mixture was then poured into different moulds and compressed with a compression moulding machine at a pressure of 30 GPa and a temperature of 350 °C. The moulds were removed from the machine and allowed to cool before the samples were detached from the moulds.

2.5 *X-ray diffraction analysis*

X-Ray Diffraction (XRD) analysis was performed using a Bruker D2-phaser X-Ray Diffraction machine with Cu Kα radiation ($\lambda = 0.154060$ nm), with a scan step of 2°/min in the 2θ range of 5° to 90°, to characterize and study the diffraction patterns of the sample powders and their phase composition.

2.6 *Fourier transform infrared spectroscopy (FTIR) analyses*

An FT-IR spectrometer (Infrared spectrometer Bruker Vertex 70 Hyperion 1000 FTIR Spectrometer) with a diamond Tttenuated Total Reflectance (ATR) accessories) was used to confirm the chemical structure of all samples and obtain information about the functional groups of the prepared HAp powders. The spectra of the samples were adjusted for background air absorbance after they were put directly into an ATR diamante crystal. Powdered samples were combined 1:100 with dry potassium bromide (KBr) to create potassium bromide (KBr) disks. At a resolution of 4 cm, the spectra were recorded in transmittance mode from 4000 to 500/400 cm^{-1}. The absorption mode was used to record the Fourier converted infrared spectra. To get the spectrum, the IR solution software was used.

2.7 *Scanning electron microscopy examination*

Scanning Electron Microscopy (SEM) using a Carl Zeiss Sigma Field Emission Gun Scanning Electron Microscope with Energy Dispersive Spectrometer (EDS) was utilized in examining the surface of the fractured samples. The samples were sputter coated with gold before examination for improved conductivity.

2.8 *Wear test*

The wear resistance test was carried out with Taber Abrasers, Model ISE-AO16 according to ASTM D4060-14 standard. This involved mounting a flat and round specimen with a diameter of approximately 100 mm and a standard thickness of approximately 3 mm to a turntable platform that rotated at a fixed speed of 150 RPM. The standard load used was 500 g. The values of the initial and final weight of the samples were used to determine the differences in the weight of each sample using the wear index. The weight loss was calculated using Equation (6) and the wear resistance was calculated according to Equation (7).

$$Weight\ loss\ (g) = Initial\ weight - final\ weight \quad (6)$$

$$Wear\ Index = \frac{W_i - W_f}{C} \times 1000 \quad (7)$$

where,

W_i - initial weight of sample,
W_f - final weight of sample, and
C - number of test cycles.

2.9 *Water absorption test*

Water absorption tests were carried out on the samples in accordance with ASTM D570-98e1. Round-shaped samples with a 40 mm diameter and 3 mm thickness were used for the experiments. To carry out the tests, clean plastic containers were procured, into which 250 cm^3 of drinking water. The initial and final weights of each sample were taken using an FA2104A chemical weighing balance. The samples were immersed in the drinking water, while readings were taken daily for 35 days. The weights gained by the samples were determined as a function of time after surface water removal.

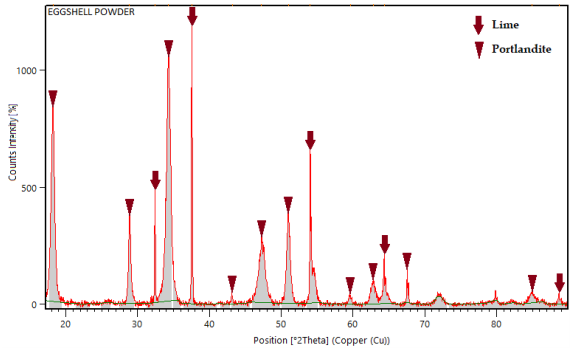

Figure 1: XRD pattern of the calcined eggshells.

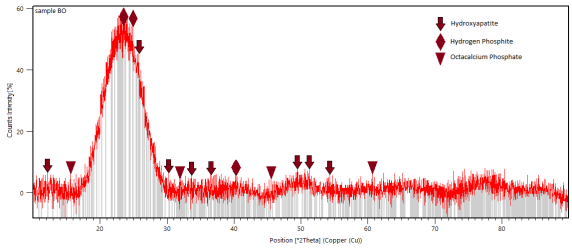

Figure 2: XRD pattern of orthophosphoric acid wet chemical precipitated eggshells

3 Results and Discussion

3.1 *X-ray diffraction*

The eggshells were found to contain Lime (CaO) with major characteristic peaks at 2θ positions 32.40°, 37.54° and 54.04°, and Calcium Hydroxide (Ca(OH)2), with minor peaks at 2θ positions 18.24°, 34.26° and 47.25°, as displayed in Figure 1, which clearly shows that lime was the most dominant phase formed although, portlandite phases were also present.

The OA-ES powders were shown in Figure 2. The XRD spectra indicated the presence of amorphous and crystalline structures. The major peak within the spectra was large and drawn out within the 2θ positions of 20° and 30° with sharp peaks at 23.37°, 24.8°, 32.4° and 34.1°, signifying the presence of hydroxyapatite, octacalcium phosphate and hydrogen phosphite peaks, respectively. The hydrogen phosphite is indicative of unreacted phosphoric acid possibly due to the rapidity of the reaction, the sharp changes in pH and other reaction kinetics. The formation of substituted or deficient apatite is very slow during simultaneous phase formation. This causes the kinetically favored phase to

form in larger proportions regardless of the fact that it possesses a smaller thermodynamic driving force. This is in agreement with the findings of Ni and Ratner, (2003) where the kinetic forces and thermodynamic factors must be balanced to ensure the formation of precursors during calcium phosphate precipitation [20]. Consequentially, this phenomenon affected the final yield. The hydroxyapatite phase formed was reduced to 66% with 12% lime and 2% portlandite while 20% consisted of other calcium and phosphorus phases. This distinction between the yield of both wet chemical precipitation methods and the generated spectra characteristics shows that the OAB-WCP is very efficient for synthesizing hydroxyapatite from eggshells.

3.2 *Fourier transformed infrared spectroscopy (FTIR)*

The chemical constituents and functional groups of the orthophosphoric acid synthesized hydroxyapatite from eggshell samples were analyzed using FTIR to identify the wave numbers and absorption refractogram obtained from FT-IR spectroscopy. Several bands, which depict the hydroxyapatite spectrum were detected as shown in Figure 3. From the spectrum of the OA-ES sample in Figure 3, a low intensity vibration band indicating the presence of hydroxyl groups from the $Ca(OH)_2$ and small amounts of water was observed at 3268.16 cm^{-1} within the range of 3200–3400 cm^{-1} associated with the O-H stretching vibration frequency, which is suggestive of dehydration and thermal breakdown during calcination [21]. The bands at 2885.02 and 2824.67 cm^{-1} are due to C–H stretching indicating carbonaceous matter within the chemical structure of the material [22]. The band at 2380.15 cm^{-1} falls within the IR spectrum around 2300 cm^{-1}, this range is affected by the absorption of CO_2 in the air [23]–[25]. The presence of carboxylic groups was also observed at 1712.99 cm^{-1} which undergo more intensive decomposition and are usually replaced by more stable compounds. Carbonate bands were observed at 1568.25 cm^{-1} indicating the presence of untransformed $CaCO_3$. A symmetric deformation mode due to v4 stretching vibration of PO_4^{3-} ion was observed at 1210.55 cm^{-1} which along with the bending of the asymmetric PO_4^{3-} characteristic band of hydroxyapatite observed at 608.02 cm^{-1} shows the presence of phosphate groups. The O-H bending and heteroatom vibration of structural O-H

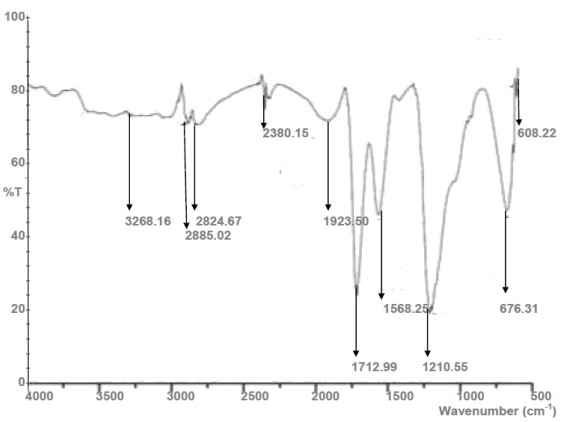

Figure 3: FT-IR spectrum of orthophosphoric acid-based wet chemical precipitated eggshell-titanium hybrid powder reinforced PEEK composite samples.

groups observed at 676.31 cm^{-1} combined with the phosphate bands and the calcium carbonate bands were all observed with minor variations in absorption band positions within the range of characteristic bands confirmed as hydroxyapatite [26]. These minor variations in the positions of absorption bands can be attributed to the presence of organic matter and trace elements, such as magnesium, potassium, iron, aluminium, silicon, and sodium within the eggshells.

3.3 *Scanning electron microscopy image*

It was observed from the SEM photomicrograph in Figure 4 that the surface of the sample after the rubbing and sliding action of the abrading wheels was characterized by a pattern of marks along the weave or grain of the material. The sample surface also revealed reinforcement particle pull-out [27]. This pull-out results in irregularly shaped cavities of varying depths and caused a disruption in the stress distribution upon loading. This behavior is a characteristic of the adhesive wear mechanism and follows the observation of Ghalme *et al.*, 2018 in which there was similar material pulling from the contact area after wear [28]. This directly influences the porosity of the material and as such its fluid absorption and retention.

3.4 *Wear behavior of the developed composites*

The wear resistance of the developed composites was

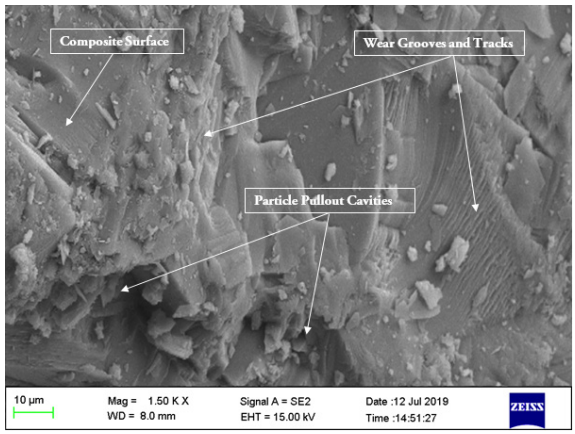

Figure 4: SEM micrograph of the abraded surface of the orthophosphoric acid-based wet chemical precipitated eggshell-titanium hybrid powder reinforced PEEK composite.

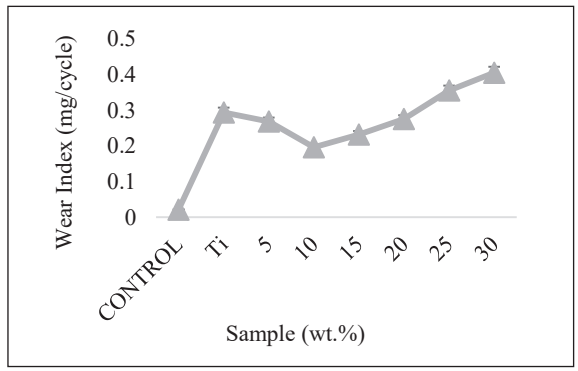

Figure 5: Effect of the derived hydroxyapatite powders and titanium powder on the wear index of the developed composites and the control sample.

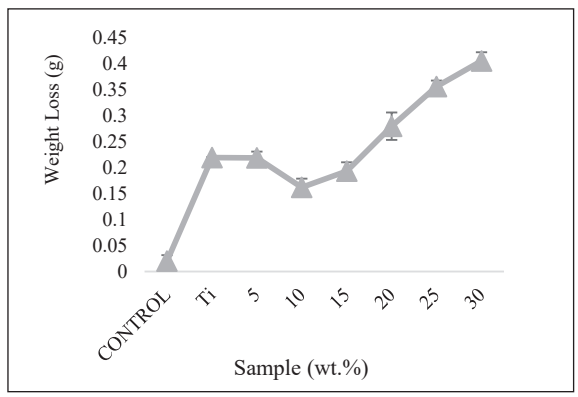

Figure 6: Effect of the derived hydroxyapatite powders and titanium powder on the weight loss of the developed composites and the control sample.

evaluated using the wear index shown in Table 5 and their weight loss. The values were plotted as shown in Figures 5 and 6, respectively. The powders from different sources influenced the wear index and weight loss in different ways. It was noticed from the results that the control sample had the lowest weight loss and the least wear index of all the samples with a value of 0.02 g and 0.0214 mg/cycle, closely followed by 10 wt.% orthophosphoric acid synthesized eggshell reinforced samples, which had the least weight loss and wear index hence, highest wear resistance of all the reinforced composite samples with a value of 0.16 g and 0.20 mg/cycle. This is in agreement with the works of Oladele *et al.*, [29]. Lower weight loss and wear index depict high wear resistance. Considering the biocompatibility of the materials, the developed biocomposites will be more suitable for the flow of body fluid as well as environmental-friendly materials. Thus, the synergy of the structural and biocompatibility requirements was achieved from a sample with 10 wt% reinforcement. Part of the reasons for the observed response from the biocomposite can be deduced from the results that the addition of HAp powders tends to increase the ploughing resistance during abrasion while fretting and sliding on the composite surface was significantly reduced. Also, this improvement could be due to the reduction in the coefficient of friction resulting from low friction force. The low frictional force has been reported to be due to the presence of natural reinforcement materials which reduced the contact area of resin to abrasion disc [30].

However, at higher HAp contents (15–30 wt.%), abrasion resistance was reduced resulting in an increase in wear rate as the HAp content was increased. These results were also in agreement with the findings of [31]. Where it was observed that for both calcined and pulverized MOFP reinforced bio-composites, the wear index increases as the reinforcement contents increase up to 12 wt.% and then decreases for both bio-composites having reinforcement contents above 15 wt.%. These observed trends could be a result of a reduction in the surface area of the binder as the filler content increases and, thus, a reduction in interfacial adhesion between the reinforcements and the matrix.

Table 5: Wear test results for five sample repetitions

Sample (wt.%)	OA-ES 1	OA-ES 2	OA-ES 3	OA-ES 4	OA-ES 5	OA-ES 1-Standard Error	OA-ES 2-Standard Error	OA-ES 3-Standard Error	OA-ES 4-Standard Error	OA-ES 5-Standard Error
Control	0.020843	0.007784	0.008487	0.007327	0.007388	0.002999	0.000691	0.000591	0.000323	0.000338
Ti	0.290938	0.2933	0.2933	0.2933	0.2933	0.000557	0.013616	0.012913	0.014073	0.014012
5	0.26787	0.2599	0.260344	0.259698	0.259735	0.000914	0.012145	0.011526	0.012462	0.01241
10	0.194007	0.185927	0.186421	0.185648	0.185687	0.00074	0.00871	0.008266	0.008912	0.008875
15	0.229403	0.219951	0.220532	0.219623	0.219668	0.002163	0.010243	0.009749	0.010522	0.010483
20	0.270875	0.25938	0.26012	0.258971	0.259026	0.002627	0.012079	0.011498	0.012407	0.012362
25	0.355044	0.3368	0.337774	0.336182	0.336264	0.00419	0.015685	0.014945	0.016094	0.016039
30	0.402101	0.404409	0.404509	0.404777	0.404762	0.000556	0.0188	0.017826	0.019418	0.019336

3.5 *Water absorption*

The water absorption results for the reinforced composites and the control are shown in Figure 7. The plots show that the addition of particulate reinforcements increases the amount of water absorbed by the composites. It was observed that the water absorption by all the composites and the control initially increased rapidly followed by a gradual increase and finally reached a saturation point where the amount of water absorbed remained constant. This was in line with Fick's Law of diffusion which relates the amount of medium flowing through a unit area of a substance per time. At the saturation stage, the composites can no longer absorb water due to the plasticizing effect of water molecules, which diffused into the matrix and reinforcement. The control sample absorbed the least amount of moisture with a saturation value of 2.59 g which implies that it is highly impermeable to water and as such more hydrophobic than the reinforced composites. The composite samples reinforced with 20 wt.% orthophosphoric acid synthesized eggshell had the highest absorption value of 6.058 g this shows that it has a high ability to absorb and retain water which implies the possibility of enhanced cell proliferation. This finding was in agreement with the report of Oladele *et al.*, [32]. The composite sample with 10 wt.% reinforcement had 3.809 g weight gain next to the control sample to emerge as the best among the composite samples with respect to moisture absorbed tendency, hence, can be considered a sample with moderate moisture absorption compared to 20 wt.% reinforced composite sample.

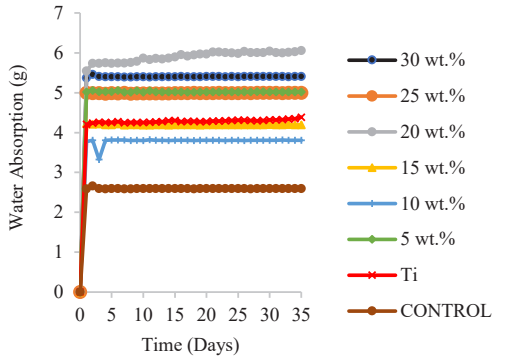

Figure 7: Water absorption results for composite samples reinforced with titanium powder and orthophosphoric acid-based wet chemical precipitated egg shell derived hydroxyapatite powders.

4 Conclusions

It was discovered from the results that the addition of blended titanium-hydroxyapatite powders to polyetheretherketone at a reinforcement content of 10 wt.% gave optimum resistance to abrasive forces with improved moisture absorption potential compared to the unreinforced polyetheretherketone. The result revealed a positive synergy of potential usage of the material with respect to abrasion resistance, porosity and density of the composite material. This ensuing characteristic brought about the possibility of a decreased in likelihood of aseptic loosening and bone necrosis. As such the composite was the best when considering both structural and biocompatibility properties. Moisture absorption of the biocomposite material was also relatively improved to ease proliferation

of bodily fluids and the resultant osseointegration of implant to the bone.

Author Contributions

A.N.: conceptualization, investigation, reviewing and editing; O.I.: investigation, methodology, writing an original draft; D.O.: research design, data analysis; A.M.: conceptualization, data curation, writing—reviewing and editing, funding acquisition, project administration. All authors have read and agreed to the published version of the manuscript.

Conflicts of Interest

The authors declare no conflict of interest.

References

[1] N. I. Agbeboh, I. O. Oladele, O. O. Daramola, A. A. Adediran, O. O. Olasukanmi, and M. O. Tanimola, "Environmentally sustainable processes for the synthesis of hydroxyapatite," *Heliyon*, vol. 6, no. 4, pp. 1–13, 2020.

[2] V. S. de Viteri and E. Fuentes, "Titanium and titanium alloys as biomaterials," in *Tribology - Fundamentals and Advancements*. London, UK: IntechOpen, 2013, p. 28.

[3] A. Sidambe, "Biocompatibility of advanced manufactured titanium implants—A review," *Materials*, vol. 7 no. 12, pp. 8168–8188, 2014.

[4] I. O. Oladele, O. G. Agbabiaka, O. G. Olasunkanmi, A. O. Balogun, and M. O. Popoola, "Non-synthetic sources for the development of hydroxyapatite," *Journal of Applied Biotechnology and Bioengineering*, vol. 5, no. 2, pp. 92–99, 2018.

[5] N. I. Agbeboh, I. O. Oladele, O. O. Daramola, A. D. Akinwekomi, M. O. Tanimola, and O. G. Olasukanmi, "Comparing the effects of two wet precipitation methods on the yield of chicken eggshell-derived hydroxyapatite," *FUTA Journal of Engineering and Engineering Technology*, vol. 16, no.1, pp. 95–104, 2022.

[6] I. O. Oladele, O. G. Agbabiaka, A. A. Adediran, A. D. Akinwekomi, and A. O. Balogun, "Structural performance of poultry eggshell derived hydroxyapatite based high density polyethylene bio-composites," *Heliyon*, vol. 5, no. 10, pp. 1–7, 2019.

[7] K. Kniha, N. Heussen, E. Weber, S. C. Möhlhenrich, F. Hölzle, and A. Modabber, "Temperature threshold values of bone necrosis for thermo-explantation of dental implants-a systematic review on preclinical in vivo research. materials," *Materials (Basel)*, vol. 13 no. 16, 2020, Art. no. 3461.

[8] J. C. M. Souza, M. S. T. Correia, B. Henriques, A. P. N. Oliveira, F. S. Silva, and J. R. Gomes, "Micro-scale abrasion wear of novel biomedical PEEK-matrix composites for restorative dentistry," *Surface Topography: Metrology and Properties*, vol. 7, no 1, 2019, Art. no. 015019.

[9] M. Reitman, D. J. Jaekel, R. Siskey, and S. M. Kurtz, *PEEK Biomaterials Handbook*, 2nd ed. Norwich, New York: William Andrew Publishing, 2019, pp. 53–66.

[10] M. Mbogori, A. Vaish, R. Vaishya, A. Haleem, and M. Javaid, "Poly-Ether-Ether-Ketone (PEEK) in orthopaedic practice- A current concept review," *Journal of Orthopaedic Reports*, vol. 1, no. 1, pp. 3–7, 2022.

[11] H. C. Alexandra, D. E. Poulsson, and R. G. Richards, "Chapter 11 - Surface modification techniques of PEEK, including plasma surface treatment," in *Plastics Design Library, PEEK Biomaterials Handbook*, S. M. Kurtz, Ed. Norwich, New York: William Andrew Publishing, 2019, pp. 179–201.

[12] T. Rajmohan, D. Kumar, and S. Manimaran, "Optimization of dry sliding wear parameters of MWCNT reinforced PolyEther-Ether-Ketone (PEEK) Composites," *Applied Mechanics and Materials*, vol. 813–814, pp. 218–225, 2015.

[13] E. Klimuszko, K. Orywal, T. Sierpinska, J. Sidun, and M. Golebiewska, "Evaluation of calcium and magnesium contents in tooth enamel without any pathological changes: in vitro preliminary study," *Odontology*, vol. 106 no.4, pp. 369–376, 2018.

[14] B. O. Asimeng, D. W. Afeke, and E. K. Tiburu, "Biomaterial for bone and dental implants: Synthesis of B-type carbonated hydroxyapatite from biogenic source," in *Biomaterials*, P. Vizureanu and C. M. D. C. F. Botelho, Eds. London, UK: IntechOpen, 2020.

[15] I. O. Oladele, O. S. Akinola, O. G Agbabiaka, and J. A. Omotoyinbo, "Mathematical model for the

prediction of impact energy of organic material based hydroxyapatite (HAp) reinforced epoxy composites," *Fibers and Polymers*, vol. 19, no. 2, pp. 452–459, 2018.

[16] N. T. Evans, F. B. Torstrick, C. S. Lee, K. M. Dupont, D. L Safranski, W. A. Chang, A. E. Macedo, A. S. Lin, J. M. Boothby, D. C. Whittingslow, R. A. Carson, R. E. Guldberg, and K. Gall, "High-strength, surface-porous polyether-ether-ketone for load-bearing orthopedic implants," *Acta Biomater*, vol. 13, pp. 159–167, 2015.

[17] A. A. Stratton-Powell, K. M. Pasko, C. L. Brockett, and J. L. Tipper, "The biologic response to polyetheretherketone (PEEK) wear particles in total joint replacement: A systematic review," *Clinical Orthopaedics and Related Research*, vol. 474, no. 11, pp. 2394–2404, 2016.

[18] O. G. Agbabiaka, I. O. Oladele, A. D. Akinwekomi, A. A. Adediran, A. O. Balogun, O. G. Olasunkanmi, and T. M. A. Olayanju, "Effect of calcination temperature on hydroxyapatite developed from waste poultry eggshell," *Scientific Africa*, vol. 8, pp. 1–12, 2020.

[19] S. A. S. Bonou, E. Sagbo, C. Aubry, C. Charvillat, B. Ben-Nissan, and S. Cazalbou, "Conversion of snail shells (Achatinaachatina) acclimatized in benin to calcium phosphate for medical and engineering use," *Journal of the Australian Ceramic Society*, vol. 55, pp. 1177–1186, 2019.

[20] M. Ni and B. D. Ratner, "Nacre surface transformation to hydroxyapatite in a phosphate buffer solution," *Biomaterials*, vol. 24, no. 23, pp. 4323–4331, 2003.

[21] S. Ferraris, S. Yamaguchi, N. Barbani, M. Cazzola, C. Cristallini, M. Miola, E. Vernèa, and S. Spriano, "Bioactive materials: In vitro investigation of different mechanisms of hydroxyapatite precipitation," *Acta Biomaterialia*, vol. 102, pp. 468–480, 2019.

[22] M. Igisu, Y. Ueno, and K. Takai, "FTIR microspectroscopy of carbonaceous matter in ~3.5 Ga seafloor hydrothermal deposits in the North Pole area, Western Australia," *Progress in Earth and Planetary Science*, vol. 5, 2018, Art. no. 85.

[23] M. Igisu, S. Nakashima, Y. Ueno, S. M. Awramik, and S. Maruyama, "In situ infrared microspectroscopy of ~850 million-year-old prokaryotic fossils," *Applied Spectroscopy*, vol. 60, pp. 1111–1120, 2006.

[24] Y. Ito and S. Nakashima, "Water distribution in low-grade siliceous metamorphic rocks by micro-FTIR and its relation to grain size: A case from the Kanto mountain region, Japan," *Chemical Geology*, vol. 189, pp. 1–18, 2002.

[25] Y. Qu, A. Engdhl, S. Zhu, V. Vajda, and N. McLoughlin, "Ultrastructural heterogeneity of carbonaceous material in ancient cherts: Investigating biosignature origin and preservation," *Astrobiology*, vol. 15, pp. 825–842, 2015.

[26] C. O. Atuanya and V. S. Aigbodion, "Effect of Wear parameters on the wear behavior of recycled low density polyethylene/snail shell biocomposites," *Journal of Failure Analysis and Prevention*, vol. 14, no. 4, pp. 509–518, 2014.

[27] S. Ghalme, A. Mankar, and Y. Bhalerao, "Integrated Taguchi-simulated annealing (SA) approach for analyzing wear behaviour of silicon nitride," *Journal of Applied Research and Technology*, vol. 15, pp. 624–632, 2018.

[28] K. V. Narasimhulu and J. L. Rao, "EPR and IR spectral studies of the seawater mussel Mytilus conradinus shells," *Spectrochim Acta A.*, vol. 56, pp. 1345–1353, 2000.

[29] I. O. Oladele, N. I. Agbeboh, B. A. Isola, and O. O. Daramola, "Abrasion and mechanical properties of keratinous based polyester composites," *Journal of Engineering and Technology*, vol. 9, no. 1, pp. 71–87, 2018.

[30] I. A. Shalwan and B. Yousif, "Influence of date palm fibre and graphite filler on mechanical and wear characteristics of epoxy composites," *Materials and Design*, vol. 59, pp. 264–273, 2014.

[31] I. O. Oladele, G. S. Ogunwande, A. S. Taiwo, and S. S. Lephuthing, "Development and characterization of Moringa Oleifera fruit waste pod derived particulate cellulosic reinforced epoxy bio-composites for structural applications," *Heliyon*, vol. 8 no. 6, pp. 1–14, 2022.